

## Original Article

# Non-isothermal kinetics of a moving phase boundary

Anna Vainchtein<sup>a</sup>

Department of Mathematics, University of Pittsburgh, Pittsburgh, PA 15260, USA

Received: November 15, 2001 / Published online September 4, 2002 – © Springer-Verlag 2002  
Communicated by Lev Truskinovsky, Minneapolis

In this paper we derive an explicit formula for a kinetic relation governing the motion of a phase boundary in a bilinear thermoelastic material capable of undergoing solid-solid phase transitions. To obtain the relation, we study traveling wave solutions of a regularized problem that includes viscosity, heat conduction and convective heat exchange with an ambient medium. Both inertia and latent heat of transformation are taken into account. We investigate the effect of material parameters on the kinetic relation and show that in a certain range of parameters the driving force becomes a non-monotone function of the interface velocity. The model also predicts a nonzero resistance to phase boundary motion, part of which is caused by the thermal trapping.

**Key words:** Non-isothermal phase transition, driving force, kinetic relation

## 1 Introduction

The complex behavior of shape memory alloys (e.g. NiTi or AgCd) has attracted a lot of attention over the past two decades, partially due to the applicability of these alloys in active structures. When subjected to applied mechanical loading, these materials undergo a martensitic phase transformation from a high-strain parent phase, called austenite, to a low-strain martensite phase. In the absence of deformation, the austenite and martensite phase are stable at high and low temperatures, respectively. The solid-solid martensitic phase transition is characterized by a lattice deformation that occurs through the correlated migration of phase boundaries. While in a certain temperature regime the transformation is reversible, i.e. upon unloading the material returns to the parent phases with little residual deformation, the *energy dissipation* associated with the motion of phase boundaries leads to a hysteretic behavior [1–4]. This remarkable property of shape memory alloys is called *pseudoelasticity*. The dynamics of phase boundaries plays an important role in the origin and size of pseudoelastic hysteresis.

Since the pioneering work of Ericksen [5], it has become common to use a non-monotone, up-down-up stress-strain relation to model the materials undergoing solid-solid phase transitions. As shown in [5], this constitutive assumption leads to an uncountable infinity of equilibrium states with piecewise-constant strain that has an arbitrary number of finite discontinuities. The corresponding dynamic initial-value problem possesses a family of solutions and thus is *ill-posed* [6]. To regularize the problem in the dynamic setting, two mechanisms have been proposed. In the first approach, called a *sharp interface theory*, an additional *kinetic relation* is postulated. This phenomenological relation expresses the jump in entropy across a phase boundary, called a *driving force*, as a function of the interface velocity and (in a thermoelastic description) temperature. For more details on this approach, see [7, 8] and references therein. As shown in these works, a kinetic relation and an additional *nucleation criterion* are sufficient to obtain a unique solution of the dynamic problem.

An alternative approach, described in [9–11], is to regularize the problem by introducing an *internal structure* in a phase boundary. This is usually accomplished by a so-called *viscosity-capillarity* model. The model includes viscous stresses of Kelvin-Voigt type, to account for internal dissipation, and a dispersive strain-gradient (capillarity) term that penalizes interface formation. Both terms introduce an internal length scale in the dynamic

<sup>a</sup>e-mail: annav@math.pitt.edu

solutions and replace the sharp interfaces by transition layers of finite thickness. By studying the traveling wave solutions for this model, one can *derive* a kinetic relation. In a suitable limit of vanishing viscosity and capillarity, this model reduces to a sharp interface theory with a *particular* kinetic relation depending on the nondimensional ratio of the length scales due to capillarity and viscosity. An additional advantage of this approach is that it does not require a separate nucleation criterion. In this model material instability automatically leads to formation of phase boundaries, which occurs via spinodal decomposition [12, 13].

This regularized theory describes the dynamics of phase boundaries in a purely mechanical (isothermal) setting. While this may be an appropriate description of quasistatic phase transitions, recent experiments on shape memory wires [2, 3] clearly indicate the influence of thermal effects, i.e. latent heat of transformation and thermal dissipation, on the overall rate of phase transition and the size and shape of pseudoelastic hysteresis at higher loading rates. To account for these effects, one-dimensional regularized models that include temperature-dependent free energy with a nonzero latent heat and thermal dissipation in the form of heat conduction, in addition to viscous dissipation and capillarity, were considered in [8, 14, 15] under the assumption that heat conductivity is large. A more general problem, with an arbitrary heat conductivity and a cubic stress-strain relation, was recently studied in [12, 16, 17], where the effect of material parameters on kinetic relations was studied numerically.

In this paper we consider a special bilinear thermoelastic material that allows us to carry out analytical calculations of traveling wave solutions for one-dimensional regularized problem that includes both viscous and thermal dissipation. The heat transfer occurs via heat conduction and convective heat exchange with the environment. We obtain an exact formula for the kinetic relation and study its dependence on the material parameters. In particular, the dependence of the driving force on temperature ahead of the front is now made explicit. In previous studies of non-isothermal kinetic relations analytical calculations were limited to either special asymptotic cases, such as infinite heat conduction [15], or approximations, e.g. neglecting latent heat term [16]. For a special case of isothermal phase transition, explicit kinetic relations have been obtained in [18] for both bilinear and cubic material laws.

Although the approach we use can equally well handle the case of nonzero strain-gradient (capillarity) coefficient, in this paper we concentrate on the special case when this coefficient is zero. There are several reasons why this limiting case, which was not previously studied in this context, is important. First, it can be shown that the model including capillarity cannot capture realistic hysteresis loops under quasistatic (isothermal) displacement-controlled loading conditions [13, 19], since there exists a range of end displacements at which single-interface solution is the only stable equilibrium. Secondly, despite the term being widely used for regularization purposes, the physical nature of the long-range atomic potentials needed for its derivation is somewhat unclear. In particular, the term results in an incorrect dispersion relation (unbounded frequencies at large wave numbers). Finally, experiment-based values of strain-gradient coefficients for shape memory alloys have never been established, and there is no evidence that such coefficients are positive for these materials, as assumed in strain-gradient models.

In the first part of the paper, we ignore the effect of convection, and thus consider a special case of the problem studied in [17] with zero capillarity and a bilinear stress-strain law. We show that when the nondimensional parameter comparing the length scales due to viscosity and heat conduction exceeds a certain threshold value, the kinetic relation becomes *non-monotone*. This result agrees with numerical observations of [17] for a cubic material and asymptotic calculations for a trilinear material [15]. In this paper we calculate the threshold parameter value above which the curves become non-monotone, and show that it is inversely proportional to the nondimensional jump in entropy due to latent heat. Non-monotone kinetic relations lead to experimentally observed [1] *stick-slip* propagation of phase boundaries, as shown in [20, 21] where non-monotonicity was postulated. In fracture mechanics, non-monotone kinetic relation, given by the dependence of fracture toughness on the crack-tip velocity, leads to the stick-slip crack-tip motion, both experimentally observed and theoretically predicted [22].

Our model also predicts nonzero *resistance* to phase boundary motion: a phase boundary cannot move until the driving force reaches a certain nonzero value. The nonzero resistance indicates nonzero energy dissipation at small interface velocities and thus is directly related to the size of quasistatic hysteresis. We emphasize that our model predicts nonzero resistance for both non-isothermal and isothermal kinetics, in contrast to the models with capillarity, which predict nonzero resistance only for the non-isothermal case [17]. In the isothermal limit, this agrees with the results of [18] which show nonzero resistance at zero capillarity. When latent heat is sufficiently high, the non-isothermal resistance is *higher* than that for the isothermal case, thus resulting in *thermal trapping* previously observed in [17] and contributing to the *thermal* portion of pseudoelastic hysteresis.

We then proceed to consider a more general model, which also includes convective heat exchange with the environment. Previous study [23, 24] of the combined effect of convection and heat conduction on a moving

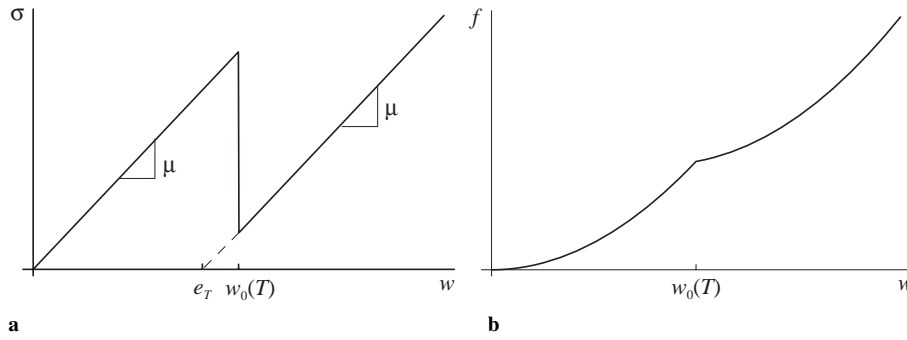


**Fig. 1. a** Bilinear stress-strain relationship  $\sigma(w, T)$ ; **b** free energy  $f(w, T)$  at fixed temperature

phase front employed a purely thermal model, based on Stefan's approach and assuming that the motion of a phase boundary is governed by the removal and supply of latent heat, while phase transformation and stress relaxation are instantaneous. The sizes of hysteresis loops predicted by these calculations are in good agreement with slow-strain-rate experiments when convection term is included. However, in the absence of convective heat exchange, the model in [23] predicts an *arbitrary* speed of interface propagation at critical stress, thus suggesting that purely thermal description is inadequate at higher loading rates, when convection effects are negligible. A more general thermomechanical description, considered in this paper, does not suffer from this deficiency. We show that when convection is included, the resistance to interface motion coincides with that for the isothermal case, but at higher velocities the kinetic relation approaches the curve for the no-convection case. Thus, the model always predicts a *finite* velocity of phase boundary. The temperature profiles agree with those obtained in [23] and show local *self-heating*, in qualitative agreement with experimental observations [2].

We show that with convection taken into account, the kinetic relation is non-monotone not only when both heat conductivity and convection coefficient are sufficiently low, but also when the latent heat is small enough. In the former case the curves are also *nonconvex*, with the absolute value of the driving force increasing at small velocities.

The structure of the paper is as follows. The model is described in Sect. 2. The procedure for finding traveling wave solutions is outlined in Sect. 3. The results for the no-convection case are discussed in Sect. 4. Section 5 is devoted to the model including convection and the resulting kinetics. Finally, Sect. 6 contains conclusions.

## 2 The model

Consider longitudinal deformations of an infinite homogeneous elastic bar of density  $\rho$ . Let  $u(x, t)$  and  $T(x, t)$  be displacement and temperature fields, respectively, at a reference point  $x$  and time  $t$ . The elastic deformation of the bar is described by the strain field  $w \equiv u_x(x, t)$ . Assume that the elastic stress in the bar is given by

$$\sigma(w, T) = \begin{cases} \mu w & \text{for } w < w_0(T) \\ \mu(w - e_T) & \text{for } w > w_0(T) \end{cases}, \quad (1)$$

see Fig. 1a. For given temperature  $T$ , the stress-strain relation (1) is a bilinear approximation of smooth non-monotone functions that are often used to model phase-transition phenomena. Bilinear stress-strain laws have been successfully employed to compute local equilibria and traveling wave solutions in the isothermal setting [18, 25]. They capture the most important features of phase transitions while enabling analytical calculations. In this case the *spinodal region* – the strain interval where stress is decreasing – degenerates into one point at which stress is discontinuous. The two strain intervals where stress is linearly increasing represent two different material phases. To simplify the calculations, we assume that both phases have the same elastic modulus  $\mu$ . The transition between two phases occurs at the strain  $w_0(T)$ . The material parameter  $e_T$ , called the *transformation strain*, denotes the distance between the linear branches. We assume that the transition strain  $w_0(T)$  increases with temperature, so that the low-strain (austenite) phase loses stability at larger deformations when temperature is higher, in agreement with experimental observations. For simplicity, we assume a linear increase:

$$w_0(T) = BT + e_T, \quad (2)$$

with  $B > 0$ . Observe that under these assumptions the *Maxwell stress* (the level of stress that divides the stress-strain graph into two regions with equal areas) is a linear function of temperature  $\sigma_M = AT + K$ , where  $A = \mu B$  and  $K = \mu e_T/2$ . The linear dependence of Maxwell stress on temperature was also assumed in [17]. Note, however, that in our model the *Maxwell strains* (the strains at which Maxwell line intersects the stress-strain graph for given temperature) linearly increase with temperature, while in [17] Maxwell strains were fixed.

The Helmholtz free energy density depicted in Fig. 1b is then given by

$$f(w, T) = -c_e T \ln \frac{T}{T_0} + \begin{cases} \frac{\mu w^2}{2} & \text{for } w \leq w_0(T) \\ \frac{\mu w^2}{2} + \mu e_T (w_0(T) - w) & \text{for } w > w_0(T). \end{cases} \quad (3)$$

Here  $c_e$  is the specific heat (assumed to be constant) and  $T_0$  is some reference temperature. Observe that the relative stability of the two phases changes with temperature, and, with  $B > 0$ , latent heat is released when low-strain phase transforms into high-strain phase. To see this, note that entropy density is

$$s(w, T) \equiv -\left. \frac{\partial f}{\partial T} \right|_w = c_e \left( 1 + \ln \frac{T}{T_0} \right) + \begin{cases} 0 & \text{for } w < w_0(T) \\ -\mu B e_T & \text{for } w > w_0(T). \end{cases} \quad (4)$$

Thus, the latent heat released during the isothermal transformation is  $Q = T(s(w_2, T) - s(w_1, T)) = -\mu B e_T T$ , where  $w_2 > w_1$  are the strains in different phases. Finally, the internal energy is given by

$$e(w, T) = f(w, T) + Ts = c_e T + \begin{cases} \frac{\mu w^2}{2} & \text{for } w < w_0(T) \\ \frac{\mu w^2}{2} + \mu e_T (e_T - w) & \text{for } w > w_0(T). \end{cases} \quad (5)$$

We consider two dissipative processes. One is thermal transport via the heat conduction, with Fourier law  $q = -\kappa T$ , where  $q$  is the heat flux and  $\kappa$  is heat conductivity. In Sect. 5 we will also consider another, convective, mode of thermal transport, but for now we ignore the effects of convection. Another dissipation mechanism is of kinetic origin. It is modeled by Kelvin-Voigt viscosity and results in the viscous stress  $\gamma u_{xt}$ , with positive viscosity coefficient  $\gamma$ . The balances of linear momentum and energy then take the following form:

$$\begin{cases} \rho u_{tt} = [\sigma(u_x, T) + \gamma u_{xt}]_x \\ (e(w, T) + \frac{1}{2} \rho u_t^2)_t = ((\sigma(w, T) + \gamma u_{xt})u_t)_x + \kappa T_{xx}. \end{cases} \quad (6)$$

Observe that the energy balance (6)<sub>2</sub> implies that

$$Ts_t = \kappa T_{xx} + \gamma u_{xt}^2. \quad (7)$$

### 3 Traveling waves

To investigate the kinetics of a phase boundary, we now seek solution to the system (6) in the form of a traveling wave:

$$u = u(z), \quad w = w(z), \quad T = T(z),$$

where  $z = x - Vt$  and  $V$  is the velocity of the wave. One can show that (6) then transform into the following dynamical system:

$$\begin{cases} w' = \frac{1}{\gamma V} [\sigma - \sigma_+ - \rho V^2 (w - w_+)] \\ T' = -\frac{V}{\kappa} [e - e_+ - \frac{1}{2} \rho V^2 (w - w_+)^2 - \sigma_+ (w - w_+)] \\ w \rightarrow w_{\pm}, \quad T \rightarrow T_{\pm}, \quad \text{as } z \rightarrow \pm\infty. \end{cases} \quad (8)$$

Here  $(w_-, T_-)$  and  $(w_+, T_+)$  are the equilibrium states behind and in front of the transition front. The constants  $\sigma_+ = \sigma(w_+, T_+)$  and  $e_+ = e(w_+, T_+)$  are the stress and internal energy density in front of the traveling front. Our objective is to obtain an exact analytical expression for the *kinetic relation*, i.e. the relationship between the *driving force*

$$G = -[[s]] = s_- - s_+ \quad (9)$$

and the velocity  $V$  of the phase boundary using the special material law (1). Observe that the entropy production rate is

$$R(V) = \int_{-\infty}^{\infty} s_t dx = -V \int_{-\infty}^{\infty} s'(z) dz = -V[[s]] = VG(V).$$

Using (7) for the entropy evolution and performing an integration by parts, one can show that

$$R(V) = \int_{-\infty}^{\infty} \left[ \kappa \left( \frac{T'}{T} \right)^2 + \gamma \frac{V^2 w'^2}{T} \right] dz \geq 0. \quad (10)$$

Thus the second law of thermodynamics is satisfied. The relations (3) and (10) imply that  $G$  and  $V$  have the same sign.

We remark that if there is an additional loss of heat  $r < 0$  per unit length, e.g. due to convective heat exchange with the environment, (7) transforms into  $Ts_t = \kappa T_{xx} + \gamma u_{xt}^2 + r$ , and total rate of entropy becomes

$$\int_{-\infty}^{\infty} s_t dx = \int_{-\infty}^{\infty} \left[ \kappa \left( \frac{T'}{T} \right)^2 + \gamma \frac{V^2 w'^2}{T} + \frac{r}{T} \right] dz. \quad (11)$$

Only the first two terms give a nonnegative contribution to (11) and are responsible for dissipation. Thus, to define the (nonnegative) entropy production rate  $R(V)$  in this case, one needs to subtract the last term in (11), yielding

$$R(V) = \int_{-\infty}^{\infty} \left( s_t - \frac{r}{T} \right) dx \geq 0$$

and the driving force given by

$$G = -[[s]] - \frac{1}{V} \int_{-\infty}^{\infty} \frac{r}{T} dz. \quad (12)$$

To reduce the number of parameters, we rescale the system (8) by using  $\mu$  as the scale of stress and energy,  $\mu/c_e$  as temperature scale,  $c = \sqrt{\mu/\rho}$  as velocity scale and  $\gamma/\sqrt{\mu\rho}$  as length scale. We then obtain the following nondimensional system:

$$\begin{cases} w' = \frac{1}{V} [\sigma - \sigma_+ - V^2(w - w_+)] \\ T' = -P_1 V [e - e_+ - \frac{1}{2} V^2(w - w_+)^2 - \sigma_+(w - w_+)] \\ w \rightarrow w_{\pm}, \quad T \rightarrow T_{\pm}, \quad \text{as } z \rightarrow \pm\infty. \end{cases} \quad (13)$$

To simplify notation, we have denoted the new nondimensional variables by the same letters as their dimensional counterparts. There are now three dimensionless material parameters:

$$P_1 = \frac{\gamma c_e}{\kappa \rho}, \quad P_2 = e_T, \quad P_3 = \frac{B\mu}{c_e}. \quad (14)$$

Here  $P_1$  is the ratio of length scales due to viscosity and heat conduction,  $P_2$  is the transformation strain and  $P_3$  is the dimensionless measure of latent heat.

Utilizing the specific expressions (1), (5) for stress and internal energy density, we can divide the problem into two. Indeed, assume that high-strain phase occupies the region  $z < 0$  and the low-strain phase is at  $z > 0$  (due to translational invariance, there is no loss of generality in assuming a phase switch at  $z = 0$ ). Then for  $z < 0$  we have

$$\begin{cases} w' = \frac{1}{V} [(1 - V^2)(w - w_+) - e_T] \\ T' = -P_1 V [T - T_+ + \frac{w^2}{2} + \frac{w_+^2}{2} + e_T(e_T - w) - \frac{1}{2} V^2(w - w_+)^2 - ww_+] \\ w \rightarrow w_-, \quad T \rightarrow T_-, \quad \text{as } z \rightarrow -\infty. \end{cases} \quad (15)$$

For  $z > 0$  the problem becomes

$$\begin{cases} w' = \frac{1}{V} (1 - V^2)(w - w_+) \\ T' = -P_1 V [T - T_+ + \frac{w^2}{2} + \frac{w_+^2}{2} - \frac{1}{2} V^2(w - w_+)^2 - ww_+] \\ w \rightarrow w_+, \quad T \rightarrow T_+, \quad \text{as } z \rightarrow +\infty. \end{cases} \quad (16)$$

In addition to solving (15) and (16), we need to impose the following jump conditions:

$$\llbracket w \rrbracket_{z=0} = 0, \quad \llbracket T \rrbracket_{z=0} = 0. \quad (17)$$

Here  $\llbracket A \rrbracket_{z=0} = A|_{z=0+} - A|_{z=0-}$  for any function  $A(z)$ . The jump conditions (17) ensure the continuity of strain and temperature. We also need to require that the phase switch occurs when  $w = w_0(T|_{z=0})$ , i.e.

$$w|_{z=0} = w_0(T|_{z=0}) = P_3 T|_{z=0} + e_T. \quad (18)$$

To complete the system of equations, we need to add the relations of the state  $(w_-, T_-)$  behind the transformation front to the state  $(w_+, T_+)$  in front of it. These are equilibria of the dynamical system (13) and satisfy the following equations:

$$\begin{cases} \sigma - \sigma_+ - V^2(w - w_+) = 0 \\ e - e_+ - \frac{1}{2}V^2(w - w_+)^2 - \sigma_+(w - w_+) = 0. \end{cases} \quad (19)$$

These equations in general imply that the equilibrium states lie at the intersections of the Rayleigh line, described by (19)<sub>1</sub>, and the Hugoniot adiabat, along which the energy balance (19)<sub>2</sub> is satisfied, in the  $(w, \sigma)$  plane [17]. For the bilinear material (1) at hand, (19)<sub>1</sub> implies that

$$w_- = w_+ + \frac{e_T}{1 - V^2}, \quad (20)$$

while (19)<sub>2</sub>, combined with (20), results in

$$T_- = T_+ + e_T \left( w_+ + \frac{e_T(V^2 - 1/2)}{1 - V^2} \right). \quad (21)$$

We now briefly describe the solution procedure. First of all, observe that due to the special material law (1), the equations (15)<sub>1</sub> and (16)<sub>1</sub> are independent of temperature. Thus in each of the phase intervals  $z < 0$  and  $z > 0$  we solve for strain  $w(z)$  first, obtaining solutions in terms of exponential functions. Next, observe that the temperature equations (15)<sub>2</sub> and (16)<sub>2</sub>, while nonlinear in  $w$ , are linear in  $T$ , due to our choice of a linear function for  $w_0(T)$ . With the formulas for  $w(z)$  now available, we solve for temperature  $T(z)$  in each interval. After applying the conditions at infinity and using (20, 21), we are left with two unknown constants. These are found from the jump conditions (17). Thus we now have exact expressions for strain and temperature as functions of  $z$ ,  $V$ ,  $w_+$  and  $T_+$ . Finally, applying the phase switch condition (18), we obtain the relation for  $w_+$  as a function of  $V$  and  $T_+$ . This relation enables us to find the desired kinetic relation  $G(V)$ . For the bilinear material the driving force defined in (9) has the form

$$G = s_- - s_+ = -P_3 e_T + \ln \left( 1 + \frac{e_T}{T_+} \left[ w_+(V, T_+) + \frac{e_T(V^2 - 1/2)}{1 - V^2} \right] \right). \quad (22)$$

#### 4 Results and discussion

In what follows, we will concentrate on the case  $V > 0$  and  $w_- > w_+$ . The calculations with negative interface velocity (in which case  $G < 0$ ) and  $w_- < w_+$  can be done in an analogous manner. Applying the solution procedure described in Sect. 3, we find that the traveling wave solution is given by

$$\begin{cases} T = T_- - \frac{P_1 V^2 (1 - V^2)}{2(P_1 V^2 + 2(1 - V^2))} (w_- - w_+)^2 e^{\frac{2(1-V^2)}{V} z} \\ w = w_- + (w_+ - w_-) e^{\frac{(1-V^2)}{V} z}. \end{cases} \quad (23)$$

at  $z < 0$  and

$$\begin{cases} T = T_+ + [T_- - T_+ - \frac{P_1 V^2 (1 - V^2)}{2(P_1 V^2 + 2(1 - V^2))} (w_- - w_+)^2] e^{-P_1 V z} \\ w = w_+. \end{cases} \quad (24)$$

at  $z > 0$ . Recall that  $T_-$  and  $w_-$  are given by (21) and (20), respectively. Applying (18), we see that  $w_+ = w_0(T|_{z=0})$  and is related to  $T_+$  and  $V$  via

$$w_+ = \frac{P_3}{1 - P_3 e_T} \left[ T_+ + \frac{e_T^2}{2(1 - V^2) + P_1 V^2} \right] + e_T. \quad (25)$$

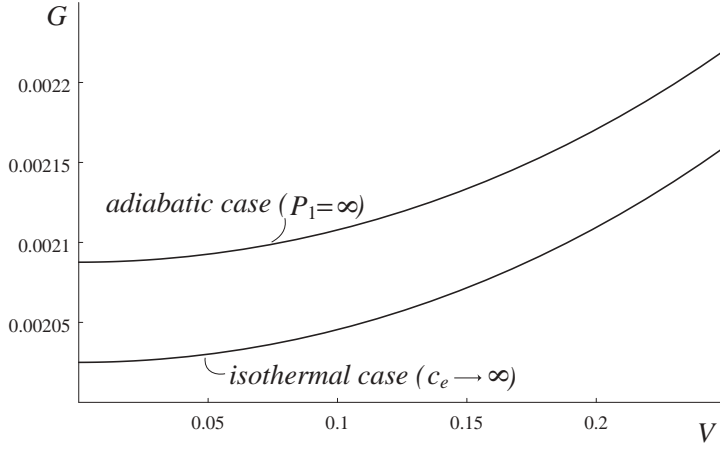


**Fig. 2.** Mobility curves  $\tilde{G}(V)$  in adiabatic ( $P_1 = \infty$ ,  $P_3 = 0.03$ ,  $c_e = 1$ ) and isothermal cases. For both curves,  $e_T = 0.45$ ,  $\tilde{T}_+ = 50$ ,  $\mu = 1$

Here and in what follows we assume that  $P_3$  is sufficiently small, so that  $1 - P_3 e_T > 0$ .

Substituting (25) in the expression (22) for the driving force, we obtain the following kinetic relation  $G(V)$  for the general non-isothermal case:

$$G(V) = -P_3 e_T + \ln \left\{ \frac{T_+ + \frac{e_T^2}{2(1-V^2)} - \frac{e_T^3 P_1 P_3 V^2}{2(1-V^2)(P_1 V^2 + 2(1-V^2))}}{(1 - e_T P_3) T_+} \right\}. \quad (26)$$

Observe that the above expressions are valid only for subsonic phase boundaries, i.e. the dimensionless velocity must satisfy  $|V| < 1$ . This is due to our choice of equal moduli for the two phases, which excludes the existence of supersonic shocks. To explain the behavior of the mobility curve  $G(V)$  in the general case for different values of material parameters  $P_1$ ,  $P_2 = e_T$  and  $P_3$ , we will consider several important special cases:

*Isothermal case* ( $c_e = \infty$ ). This purely mechanical model has been extensively studied (see, for example, [18], where exact formulas are obtained for bilinear and cubic stress-strain relations, and references therein). It assumes infinite specific heat  $c_e$ . To obtain this limit of our non-isothermal model, consider the unrescaled energy balance (8)<sub>2</sub>. Recalling that the internal energy density has the form  $\tilde{e}(w, \tilde{T}) = c_e \tilde{T} + g(w)$  in each phase region, one can rewrite (8)<sub>2</sub> as

$$\tilde{T}' = -\frac{\tilde{V}}{\kappa} [c_e(\tilde{T} - \tilde{T}_+) + g(w) - g(w_+) - \frac{1}{2} \rho \tilde{V}^2 (w - w_+)^2 - \tilde{\sigma}_+(w - w_+)].$$

Here  $\tilde{T} = (\mu/c_e)T$ ,  $\tilde{V} = cV$  and  $\tilde{\sigma} = \mu\sigma$  denote the original dimensional temperature, velocity and stress. Thus, in the isothermal limit of  $c_e \rightarrow \infty$ , this equation yields  $\tilde{T} = \tilde{T}_+$ . The problem now reduces to a single equation which coincides with (13)<sub>1</sub> in the dimensionless form. In the isothermal case the (dimensional) driving force reduces to

$$\tilde{G} = \frac{\mu}{\tilde{T}_+} \left( f_+ - f_- - \frac{\sigma_+ + \sigma_-}{2} (w_+ - w_-) \right). \quad (27)$$

For our bilinear material (27) yields

$$\tilde{G}(V) = \frac{\mu e_T^2}{2\tilde{T}_+(1-V^2)} \quad (28)$$

at  $V > 0$ , which coincides with the results of [18] for zero capillarity. The mobility curve is the lower line depicted in Fig. 2. Observe that  $\tilde{G}(V)$  is a monotone function in this case. Notice also that  $\tilde{G}(0+) > 0$ , so that a nonzero driving force is needed for the boundary to start moving. This feature contributes to the *isothermal hysteresis* observed in shape-memory-alloy wires at quasistatic (extremely slow) loading.

By recalling (14) and expanding (26) for large  $c_e$ , it is easy to see that the driving force for the non-isothermal case takes the form

$$\tilde{G} = c_e G = \frac{\mu e_T^2}{2\tilde{T}_+(1-V^2)} + O\left(\frac{\mu^2 B}{c_e \tilde{T}_+}\right).$$

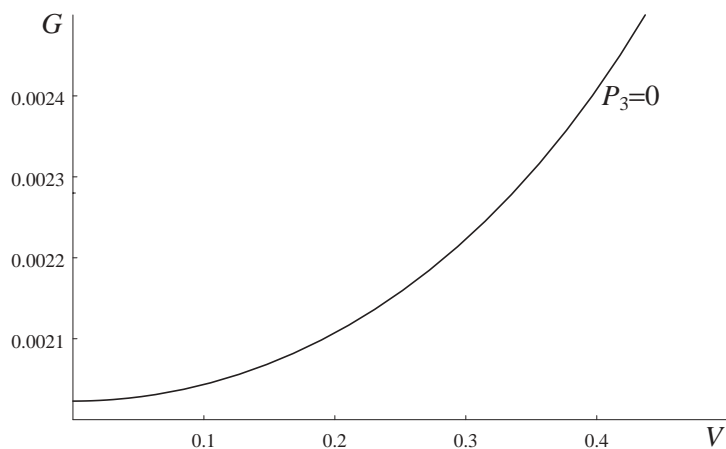


**Fig. 3.** Dimensionless mobility curve  $G(V)$  for the case of zero latent heat:  $P_3 = 0$ ,  $e_T = 0.45$ ,  $T_+ = 50$

Thus, (28) approximates (26) for large  $c_e$ .

*Zero latent heat ( $B = 0$ ).* In some cases, for example, during twinning, no heat is released during a phase transition. Thus  $B = 0$  and hence  $P_3 = 0$ . In this special case the transitional strain  $w_0 = e_T$  is temperature-independent. The formulas (23) and (24) still hold, but (25) reduces to  $w_+ = e_T$ . Note that the process is not isothermal due to the combination of nonzero viscous dissipation and finite heat conduction. The nondimensional driving force reduces to

$$G(V) = \ln \left\{ 1 + \frac{e_T^2}{2(1 - V^2)T_+} \right\}, \quad (29)$$

which is a monotone function of  $V$ . Observe that it is independent of  $P_1$ . The mobility curve is shown in Fig. 3.

*“Almost isothermal” case: infinite heat conductivity ( $P_1 = 0$ ).* This asymptotic case was studied in [14] and [26] in the context of the van der Waals fluids. Kinetic relations for this limit were obtained in [15] and [16, 17] for trilinear and cubic materials, respectively, for the models including strain-gradient (capillarity) terms. As first shown in [14], in this case the actual phase transition occurs almost isothermally in the region whose width scales with  $\gamma/\sqrt{\mu\rho}$  (the length scale we have chosen). The redistribution of latent heat takes place in a much larger thermal boundary layer of width proportional to  $\kappa/(c_e c)$ , where  $c = \sqrt{\mu/\rho}$  is the isothermal sound speed. To see this and check our general solution, one can obtain the inner asymptotic expansion by putting  $P_1 = 0$  in the equations (13)<sub>1,2</sub>. This yields

$$\begin{cases} w' = \frac{1}{V}[\sigma - \sigma_+ - V^2(w - w_+)] \\ T' = 0 \\ w \rightarrow w_-, \quad T \rightarrow T_- \quad \text{as } z \rightarrow -\infty \\ w \rightarrow w_B \quad \text{as } z \rightarrow \infty. \end{cases} \quad (30)$$

Here  $w_B$  is the value of strain at the boundary with the thermal layer. Thus on the length scale of  $\gamma/\sqrt{\mu\rho}$  the phase transition from  $w_-$  to  $w_B$  occurs isothermally, with  $T = T_-$ . To obtain the outer expansion, rescale (13) with  $\bar{z} = P_1 z$ :

$$\begin{cases} P_1 w' = \frac{1}{V}[\sigma - \sigma_+ - V^2(w - w_+)] \\ P_1 T' = -P_1 V[e - e_+ - \frac{1}{2}V^2(w - w_+)^2 - \sigma_+(w - w_+)] \\ w \rightarrow w_B, \quad T \rightarrow T_-, \quad \text{as } \bar{z} \rightarrow -\infty \\ w \rightarrow w_+, \quad T \rightarrow T_+, \quad \text{as } \bar{z} \rightarrow \infty. \end{cases}$$

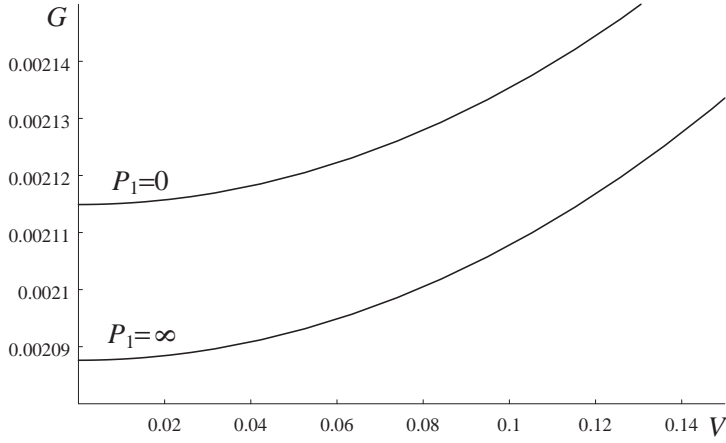


**Fig. 4.** Dimensionless mobility curves  $G(V)$  for the cases  $P_1 = 0$  and  $P_1 = \infty$ . Other parameters:  $P_3 = 0.03$ ,  $e_T = 0.45$ ,  $T_+ = 50$

For small  $P_1$  this becomes

$$\begin{cases} \sigma - \sigma_+ - V^2(w - w_+) = 0 \\ T' = -V[e - e_+ - \frac{1}{2}V^2(w - w_+)^2 - \sigma_+(w - w_+)] \\ w \rightarrow w_B, \quad T \rightarrow T_-, \quad \text{as } \bar{z} \rightarrow -\infty \\ w \rightarrow w_+, \quad T \rightarrow T_+, \quad \text{as } \bar{z} \rightarrow \infty. \end{cases} \quad (31)$$

Thus in the thermal layer the trajectory follows the Rayleigh line (31)<sub>1</sub>, while the temperature changes from  $T_-$  to  $T_+$  according to (31)<sub>2</sub>. Combining (30, 31) with (18, 19) and enforcing the continuity of  $w$  at  $z = 0$ , one can show that

$$w_+ = w_B = \frac{P_3}{1 - P_3 e_T} \left\{ T_+ + \frac{e_T^2}{2(1 - V^2)} \right\} + e_T.$$

Hence the driving force is

$$G = -P_3 e_T + \ln \frac{1 + \frac{e_T^2}{2(1 - V^2)T_+}}{1 - P_3 e_T}, \quad (32)$$

which agrees with (26) when  $P_1 = 0$ . See the mobility curve (upper line) in Fig. 4.

*Zero heat conduction* ( $P_1 = \infty$ ). In this case the process is adiabatic everywhere. Assume, as above, that  $V > 0$ . Then (13)<sub>2</sub> reduces to the algebraic equation

$$e - e_+ - \frac{1}{2}V^2(w - w_+)^2 - \sigma_+(w - w_+) = 0$$

that can be solved for temperature:

$$T = \begin{cases} T_+ - \frac{w^2}{2} - e_T(e_T - w) + \frac{w_+^2}{2} + \frac{1}{2}V^2(w - w_+)^2 + w_+(w - w_+) & \text{at } z < 0 \\ T_+ - \frac{w^2}{2} + \frac{w_+^2}{2} + \frac{1}{2}V^2(w - w_+)^2 + w_+(w - w_+) & \text{at } z > 0. \end{cases} \quad (33)$$

Observe that in this case the temperature has a finite jump discontinuity  $\llbracket T \rrbracket = e_T^2$  at  $z = 0$ . This is caused by the degeneracy of the bilinear model which results in entropy and hence internal energy being discontinuous at the phase switch. Solving for strain in both phases, we have

$$w = \begin{cases} w_+ + \frac{e_T}{1 - V^2}(1 - e^{\frac{1-V^2}{V}z}) & \text{at } z < 0 \\ w_+ & \text{at } z > 0. \end{cases} \quad (34)$$

Substituting this in (33) and enforcing  $w|_{z=0-} = e_T + P_3 T|_{z=0-}$ , one obtains

$$w_+ = \frac{e_T + P_3(T_+ - e_T^2)}{1 - P_3 e_T}. \quad (35)$$

The driving force is then given by

$$G = -P_3 e_T + \ln \frac{T_+ + e_T \left\{ \frac{e_T + P_3(T_+ - e_T^2)}{1 - P_3 e_T} + \frac{e_T(V^2 - 1/2)}{1 - V^2} \right\}}{T_+}. \quad (36)$$

The mobility curve is shown in Figs. 2, 4. Similar to the isothermal and ‘‘almost isothermal’’ cases,  $G$  is a monotone function of  $V$ .

In the limit  $V \rightarrow 0+$ , (34) yields a discontinuous strain profile

$$w \rightarrow \begin{cases} w_- = w_+ + e_T & \text{at } z < 0 \\ w_+ & \text{at } z > 0 \end{cases}$$

with constant stress, where  $w_+$  is given by (35). Meanwhile, the temperature limit becomes

$$T \rightarrow \begin{cases} T_- = \frac{T_+}{1 - P_3 e_T} + \frac{e_T^2}{2} > T_+ & \text{at } z < 0 \\ T_+ & \text{at } z > 0. \end{cases}$$

Thus at  $\kappa = 0$  and  $V \rightarrow 0+$  the temperature is discontinuous at  $z = 0$ , with the finite jump depending on  $P_3$ ,  $T_+$  and  $e_T$ . We emphasize that not all of the jump is due to the degeneracy of the model. Indeed, the temperature behind the discontinuity is *higher* than the temperature in front because in the absence of heat conduction the system is unable to remove the latent heat of transformation and equilibrate the temperature. This leads to the *thermal trapping* effect first observed in [17]. In order for a phase boundary to start moving, a nonzero driving force

$$G_r = G(0+) = -P_3 e_T + \ln \left( \frac{1}{1 - P_3 e_T} + \frac{e_T^2}{2T_+} \right) \quad (37)$$

is needed. This initial driving force is called *resistance* to interface motion. At finite  $c_e$  and  $P_3$  exceeding a certain threshold value  $P_3^a$ , the value of resistance for the adiabatic case is *larger* than its value

$$G_r = \frac{e_T^2}{2T_+}$$

for the isothermal case<sup>1</sup> and approaches the isothermal limit as  $c_e \rightarrow \infty$ . See Fig. 5. This additional driving force is thus due to the thermal effects and may contribute to the thermal portion of the hysteresis loop.

*General case.* Now consider the general non-isothermal case. Recall that the kinetic relation is given by (26). We will concentrate on the effect of three thermal parameters:  $P_1$ ,  $P_3$  and  $T_+$  on the mobility curves.

We begin by considering the effect of  $P_1$ . Recall from (14) that this parameter compares the length scales due to viscosity and heat conduction. We have already seen the mobility curves for the two extreme cases,  $P_1 = 0$  and  $P_1 = \infty$  (Fig. 4). The mobility curves for the general case of finite  $P_1$  are shown in Fig. 6. One can see that when  $P_1$  is sufficiently small, the curves are monotonically increasing functions of  $V$ . As  $P_1$  increases, the mobility curves shift downward because the decrease in thermal dissipation at smaller heat conductivity lowers the driving traction needed to maintain the same velocity of the front. As  $P_1$  exceeds a certain critical value (depending on  $P_3$ ), the curves become *non-monotone*. For  $P_1$  above this threshold, the driving force first *decreases* and then increases with growing  $V$ . To see the reason for the non-monotonic kinetic relations, observe that all curves with finite nonzero  $P_1$  start at the same point, with resistance

$$G_r = G(0+) = -P_3 e_T + \ln \left\{ \frac{T_+ + \frac{e_T^2}{2}}{(1 - e_T P_3) T_+} \right\}. \quad (38)$$

<sup>1</sup> For the purpose of comparing non-isothermal and isothermal kinetics, here and in what follows we normalize the temperature and driving force in the isothermal case using the finite specific heat  $c_e$  of the non-isothermal problem.

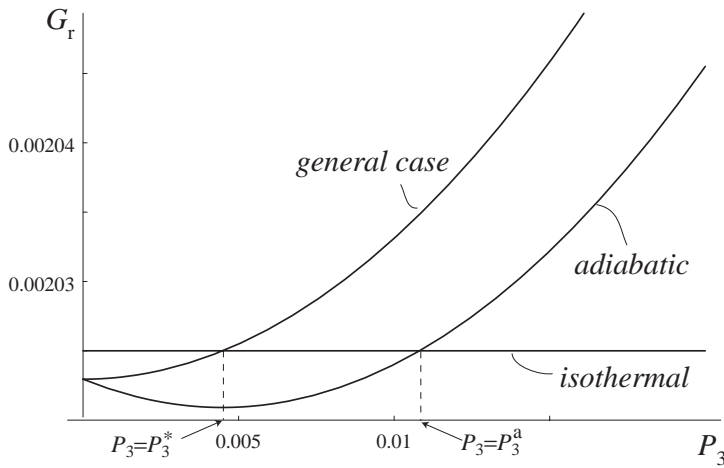


**Fig. 5.** Effect of  $P_3$  on the resistance  $G_r$  to interface motion for the adiabatic, isothermal and general non-isothermal cases. Other parameters:  $e_T = 0.45, T_+ = 50$

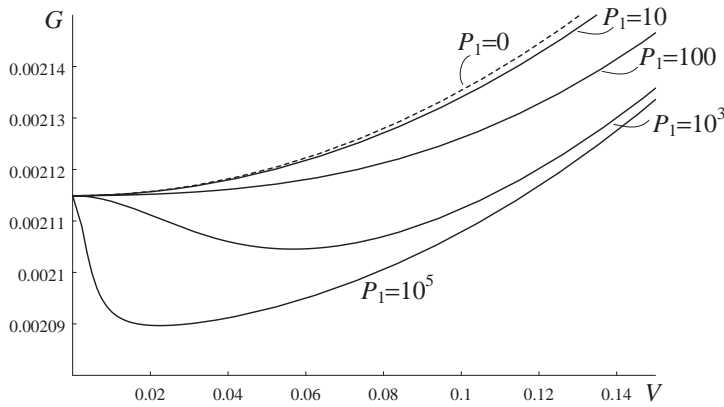


**Fig. 6.** Effect of  $P_1$  on the mobility curve  $G(V)$  for the general non-isothermal case. Other parameters:  $P_3 = 0.03, e_T = 0.45, T_+ = 50$

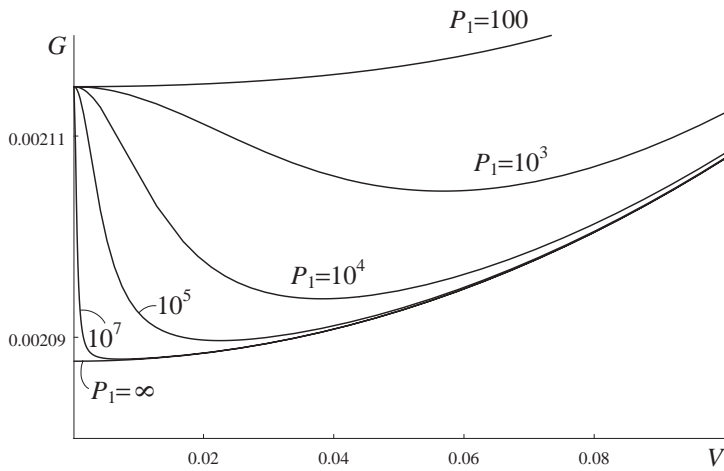


**Fig. 7.** The mobility curve  $G(V)$  for the general non-isothermal case at large  $P_1$ . Other parameters:  $P_3 = 0.03, e_T = 0.45, T_+ = 50$

But as the interface velocity increases, the curves approach the mobility curve for the adiabatic case. This is especially clear from Fig. 7 which shows the curves at large  $P_1$  together with the curve for the adiabatic case. Indeed, when the interface is moving sufficiently fast at given  $P_1$ , the system does not have time to redistribute the heat. Thus, the process is increasingly close to adiabatic as  $V$  grows. The smaller heat conductivity (the larger  $P_1$ ), the smaller the velocity of the front at which the transition to the quasi-adiabatic regime occurs. As the interface slows down, there is more time to redistribute temperature. Thus, as  $V$  becomes smaller, the kinetic relation approaches the mobility curve for the “almost isothermal” case  $P_1 = 0$ . The latter curve is higher than the curve for the adiabatic limit. This causes the non-monotonicity of the mobility curves at sufficiently large  $P_1$ .

We can take advantage of the availability of an exact formula (26) for the kinetic relation and find the threshold value of  $P_1$  above which the curves become non-monotone. We find that the non-monotonicity takes place for

$$P_1 > \frac{2}{e_T P_3}. \quad (39)$$

So the higher is  $P_3$  (e.g. larger latent heat or smaller specific heat), the lower is the threshold value  $P_1^*$  above which the curves lose their monotonicity.

The fact that kinetic curves become non-monotone when heat conductivity is sufficiently low confirms the numerical observations of [17] for a non-isothermal viscosity-capillarity model. In fact, as the asymptotic calculations for a trilinear material [15] have shown, when capillarity (strain-gradient) term  $\frac{1}{2}\varepsilon^2 w_x^2$  is included in the free energy (3), the mobility curve is non-monotone even in the case when  $P_1$  is small, provided that viscosity is small relative to capillarity:  $\gamma/\varepsilon\sqrt{\rho} \ll 1$ . Similar non-monotonicity was also observed in [27,28] for a related non-isothermal Ginzburg-Landau model. This result is interesting in view of the papers [20,21], where a postulated non-monotone kinetic relation led to a *stick-slip* interface motion. Such kinetics is often called *unstable* because the non-monotonicity of the kinetic relation leads to the nonconvexity of the entropy production rate  $R(V) = GV$ , and thus the traveling waves corresponding to the decreasing portion of the mobility curve are probably unstable. In fact, numerical calculations of [16,17] show the existence of multiple branches (loops) of traveling wave solutions at small  $V$  for non-monotone  $G(V)$ . In these solutions strain and temperature oscillate within the transition region. To compute the loop structure for the present model, one needs to assume that phase switches occur at several unknown locations  $z = c_i$ , in addition to  $z = 0$ , and enforce (18) at each of these. The problem then reduces to solving a system of nonlinear algebraic equations for  $c_i$ . These calculations will be presented elsewhere.

Another important observation is the thermal trapping phenomenon. We have already mentioned this effect when the adiabatic case was discussed. One can see that it also takes place in the general non-isothermal setting. In fact, in the general case with nonzero  $P_3$ , the resistance  $G_r$ , given by (38), is always higher than the initial force needed in the adiabatic setting. At  $P_3$  above the threshold value  $P_3^* < P_3^a$ , it is also higher than  $G_r$  for the isothermal motion (see Fig. 5). To see this more clearly, consider the limit  $V \rightarrow 0$ . Using an asymptotic expansion similar to the case  $P_1 \rightarrow 0$ , one can show that in this limit the phase transition occurs isothermally in the region scaling with  $V$ , while the heat is redistributed in the adjacent thermal layer of a much larger width. Indeed, at small  $V$  (13)<sub>1,2</sub> can be approximated by (inner expansion)

$$\begin{cases} w' = \frac{1}{V}(\sigma(w, T) - \sigma_+) \\ T' = 0. \end{cases} \quad (40)$$

Thus the first segment of the singular trajectory is isothermal, with  $T = T_-$  and

$$w(z) = \begin{cases} w_+ + e_T(1 - e^{z/V}) & \text{for } z < 0 \\ w_+ & \text{for } z > 0. \end{cases} \quad (41)$$

As  $V \rightarrow 0+$ , the strain profile tends to the discontinuous equilibrium

$$w(z) = \begin{cases} w_- = w_+ + e_T & \text{for } z < 0 \\ w_+ & \text{for } z > 0, \end{cases} \quad (42)$$

with  $\sigma = \sigma_- = \sigma_+$ . From (21) one can see that  $T_- = T_+ + e_T(w_+ - e_T/2) > T_+$ . To obtain the equations governing the behavior in the thermal (outer) layer, we rescale (13) using  $\bar{z} = Vz$  and put  $V = 0$ . This results in

$$\begin{cases} \sigma = \sigma_+ \\ T' = -P_1[e - e_+ - \sigma_+(w - w_+)] \\ w \rightarrow w_+, \quad T \rightarrow T_+, \quad \text{as } \bar{z} \rightarrow \infty. \end{cases} \quad (43)$$

Hence in the second segment of the small- $V$  trajectory  $w = w_+$  and the temperature decreases to  $T_+$  according to (43)<sub>2</sub>. Going back to the original variable  $z = \bar{z}/V$ , we see that

$$T(z) = \begin{cases} T_- & \text{for } z < 0 \\ (T_- - T_+)e^{-P_1 Vz} + T_+ & \text{for } z > 0. \end{cases} \quad (44)$$

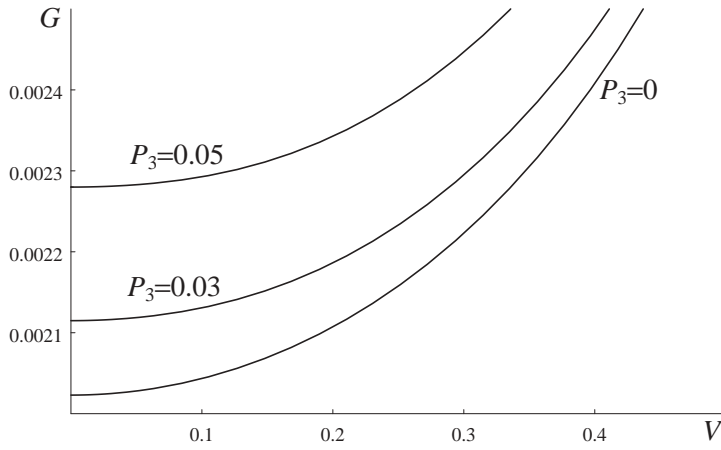


**Fig. 8.** The effect of  $P_3$  on the mobility curve  $G(V)$  for the general non-isothermal case. Other parameters:  $P_1 = 40$ ,  $e_T = 0.45$ ,  $T_+ = 50$

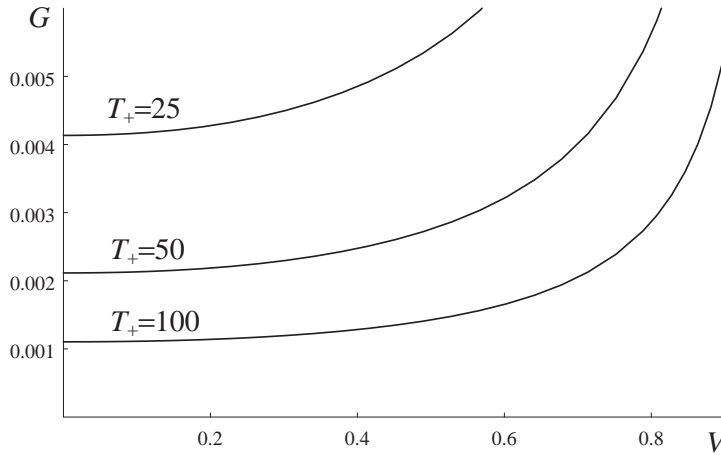


**Fig. 9.** The effect of  $T_+$  on the mobility curve  $G(V)$  for the general non-isothermal case. Other parameters:  $P_1 = 40$ ,  $e_T = 0.45$ ,  $P_3 = 0.03$

The continuity of  $w$  at  $z = 0$  and the phase-switch condition (18) together imply that  $w_+ = w_0(T_-)$ , and thus

$$T_- = \frac{T_+ + \frac{e_T^2}{2}}{1 - P_3 e_T}. \quad (45)$$

As  $V \rightarrow 0+$ , (44) yields  $T \rightarrow T_-$  for all  $z$ . Hence as interface slows down, the bar reaches an equilibrium, and the temperature field becomes uniform and given by (45). Observe that  $T_-$  is higher than  $T_+$ , the temperature the bar would have at zero velocity under isothermal assumption. This overall heating increases the value of the transformation stress and, at sufficiently high values of  $P_3$  ( $P_3 > P_3^*$ ), requires a *higher* initial driving traction (38) than is needed in the isothermal case. At large specific heat, one can estimate the threshold value  $P_3^*$  by expanding (38) in Taylor series. This yields

$$P_3^* \approx \frac{e_T}{2T_+}. \quad (46)$$

Recall that in the adiabatic case ( $P_1 = \infty$ ) only the temperature behind the boundary increases, while the temperature in front remains equal to  $T_+$ , due to the absence of thermal dissipation. Hence the resistance to interface motion in this case is lower than in the general non-isothermal setting. Observe also that the value of  $G_r$  is independent of  $P_1$  and depends only on  $P_2 = e_T$ ,  $P_3$  and  $T_+$ .

The effect of  $P_3$ , the parameter controlling the latent heat, is shown in Fig. 8. One can see that the curves shift up as  $P_3$  is increased. Hence thermal trapping is more pronounced at higher  $P_3$ .

Finally, Fig. 9 shows the effect of  $T_+$  on the mobility curves. As the temperature in front of the transformation front decreases, the driving force for given  $V > 0$  grows. Note that the function  $V = H(G, T_+)$ , obtained by inverting (26), is nontrivial and in general not single-valued.

## 5 Kinetics with convection

The calculations we have presented so far apply to an idealized situation in which heat conduction is the only mode of heat transfer. This is a good approximation for kinetics of a phase transition under adiabatic conditions, for example, when a specimen is tested at high loading rates, is well isolated or put in a relatively non-convective environment, such as air. A more realistic model should include heat convection as another important mode of heat transfer. Indeed, experiments [2, 3] have shown a significant difference in the size of hysteresis loops for specimens tested in water (which has a high convection coefficient) and air. To take this effect into account, we assume a heat loss

$$r = -\eta(T - T_+) \quad (47)$$

through the lateral surface of the bar. Here  $\eta = 2h/r_0$  is the convection coefficient  $h$  normalized by the radius  $r_0$  of the circular cross-section of the bar. With this assumption, the energy balance (13)<sub>2</sub> transforms into

$$T'' = P_1 V [(\sigma(w, T) - V w') w - e(w, T) - \frac{1}{2} V^2 w^2]' + P_4 (T - T_+), \quad (48)$$

where

$$P_4 = \frac{\eta \gamma^2}{\mu \rho \kappa} \quad (49)$$

is the new nondimensional parameter. Adopting the bilinear material, we have

$$T'' + P_1 V T' - P_4 (T - T_+) = -P_1 V [V w w' - \frac{1}{2} (1 - V^2) w^2]' + P_1 V e_T^2 \delta(z). \quad (50)$$

Here  $\delta(z)$  is the Dirac delta function. The linear momentum balance (13)<sub>1</sub> does not change. As before, we need to enforce continuity of strain and temperature and the phase switch condition (18) at  $z = 0$ . An additional condition on the jump of the temperature gradient,

$$[[T']]_{z=0} = P_1 V (e_T^2 - V w_0(T(0))) [[w']]_{z=0}, \quad (51)$$

follows from integrating (50).

The solution is then found to have the following form. The strain profile is given by

$$w(z) = \begin{cases} w_+ + \frac{e_T}{1 - V^2} (1 - e^{\frac{1-V^2}{V} z}) & \text{for } z < 0 \\ w_+ & \text{for } z > 0, \end{cases} \quad (52)$$

while the temperature is

$$T(z) = \begin{cases} T_+ + C_2 e^{\lambda_1 z} - C_1 e^{\frac{2(1-V^2)}{V} z} & \text{for } z < 0 \\ T_+ + C_3 e^{\lambda_2 z} & \text{for } z > 0. \end{cases} \quad (53)$$

Here we define

$$\lambda_{1,2} = \frac{-P_1 V \pm \sqrt{P_1^2 V^2 + 4P_4}}{2}, \quad (54)$$

so that  $\lambda_1 > 0$  and  $\lambda_2 < 0$ . The constants  $C_1$ ,  $C_2$  and  $C_3$  are given by the following formulas:

$$C_1 = \frac{P_1 V^2 e_T^2}{4(1 - V^2)^2 + 2P_1 V^2(1 - V^2) - P_4 V^2}, \quad (55)$$

$$C_2 = \phi(V) \left\{ \frac{e_T^2 [4(1 - V^2) + P_1 V^2(1 - 2P_3 e_T) + V \sqrt{P_1^2 V^2 + 4P_4}]}{2[4(1 - V^2)^2 + 2P_1 V^2(1 - V^2) - P_4 V^2]} + P_3 e_T T_+ \right\} \quad (56)$$

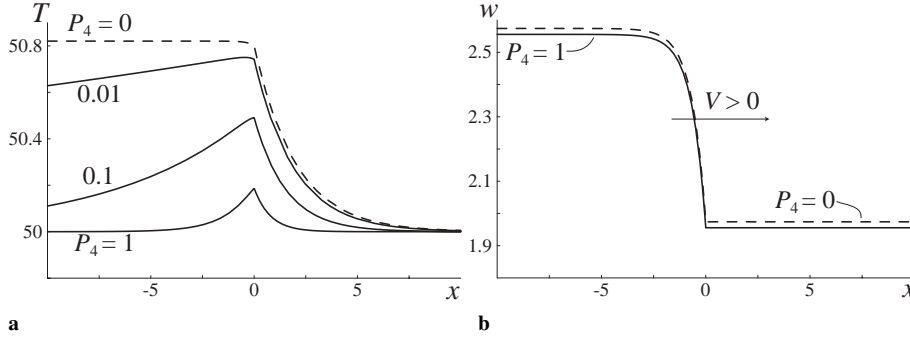


**Fig. 10.** **a** Temperature and **b** strain profiles of the traveling wave at  $V = 0.5$  and different values of the convection parameter  $P_4$ . Other parameters:  $P_1 = 1$ ,  $P_2 = e_T = 0.45$ ,  $P_3 = 0.03$

and

$$C_3 = \phi(V) \left\{ \frac{e_T^2 [4(1-V^2) + P_1 V^2 - V \sqrt{P_1^2 V^2 + 4P_4}]}{2[4(1-V^2)^2 + 2P_1 V^2(1-V^2) - P_4 V^2]} + P_3 e_T T_+ \right\}, \quad (57)$$

where

$$\phi(V) = \frac{P_1 V}{\sqrt{P_1^2 V^2 + 4P_4} - P_3 P_1 V e_T}.$$

Typical temperature and strain profiles for several values of  $P_4$  are depicted in Fig. 10. Observe that the states at  $z \rightarrow \pm\infty$  now both have temperature  $T_+$ , so that  $T_- = T_+$  in this case. Note, however, the peaks in temperature profiles at the phase switch location  $z = 0$ . These peaks are mostly due to the latent heat of transformations. Local heating at the site of transformation front are experimentally observed [2, 3]. As the parameter  $P_4$  is decreased to zero, the peaks increase, and the temperature decreases to  $T_+$  as  $z \rightarrow -\infty$  at a slower rate. This qualitatively agrees with experimental observations of a more substantial self-heating when the specimen is tested in a less convective environment [3]. We remark that in a model with a non-degenerate spinodal region the cusps would smoothen out but the peaks would remain.

Enforcing the phase-switch condition (18), we have  $w_+ = e_T + P_3(T_+ + C_3)$ . Using (12), one can show that the driving force in this case is given by

$$G = -[[s]] + \frac{P_4}{P_1 V} \int_{-\infty}^{\infty} \frac{T - T_+}{T} dz, \quad (58)$$

where we have taken heat loss due to convection into account. This expression can be further reduced to

$$G = -P_3 e_T + \frac{\sqrt{P_1^2 V^2 + 4P_4}}{P_1 V} \ln\left(1 + \frac{C_3}{T_+}\right) - \frac{P_4(\nu - 1)}{\lambda_1 V P_1} \int_0^1 \frac{dt}{R - t + Qt^\nu}. \quad (59)$$

Here  $\nu = \lambda_1 V / (2(1 - V^2))$ ,  $R = T_+ / C_1$  and  $Q = C_2 / C_1$ . We were unable to find an analytical expression for the integral in the last term, so it was evaluated numerically.

The resulting mobility curves are shown in Fig. 11 for both small and large values of  $P_1$ . One can see that for all curves the resistance  $G_r = G(0+)$  coincides with the initial driving force for the isothermal curve, shown in Fig. 11 as a dashed line. Indeed, as velocity of the boundary tends to zero, the convection forces the temperature in the bar to approach the uniform profile  $T = T_+$ . However, as  $V$  increases, the mobility curves approach the curve for  $P_4 = 0$  (no convection) case. Thus, at faster propagation of the transition front the convection mechanism becomes less important, and the model that contains heat conduction as the only mechanism of thermal dissipation ( $P_4 = 0$ ) becomes more reasonable. In fact, at high enough  $V$ , the mobility curves approach the curve for the adiabatic case ( $P_1 = \infty$ ) in models both with and without convection. This happens because of the inability of the system to redistribute and dissipate heat when a phase boundary is moving fast enough.

The mobility curves are also affected by the amount of latent heat measured by  $P_3$ . As Fig. 12a shows, when  $P_3$  is below the threshold value  $P_3^*$ , approximated by (46), the isothermal curve is *above* the  $P_4 = 0$  curve (and the adiabatic curve) at small  $V$ . As described above, the curves with nonzero  $P_4$  always start at the isothermal resistance value. In this case the driving force *initially decreases* with growing  $V$  and then increases again,

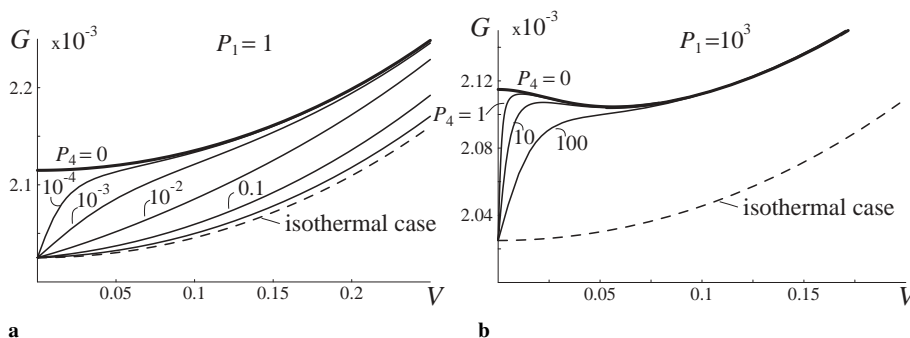


**Fig. 11.** Effect of the convection parameter  $P_4$  on the mobility curves  $G(V)$  at (a)  $P_1 = 1$ , (b)  $P_1 = 10^3$ . Other parameters:  $P_2 = e_T = 0.45$ ,  $P_3 = 0.03$ . The curves are shown together with the curves for the isothermal case (dashed line) and  $P_4 = 0$  case (upper curve)

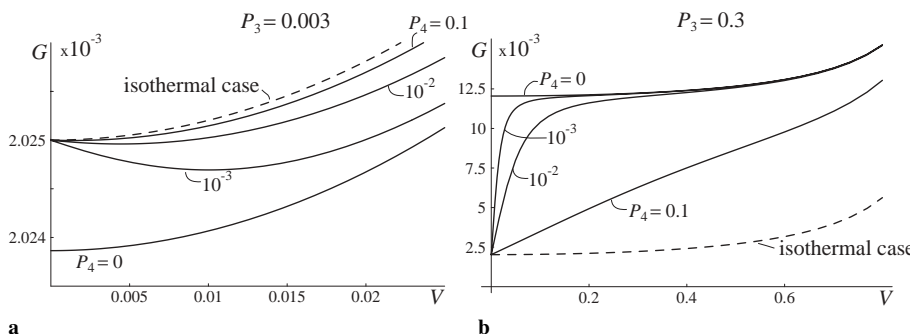


**Fig. 12.** Effect of the convection parameter  $P_4$  on the mobility curves  $G(V)$  at a  $P_3 = 0.003 < P_3^*$ , b  $P_3 = 0.3 > P_3^*$ . Other parameters:  $P_1=1$ ,  $P_2 = e_T = 0.45$ . In this case  $P_3^* \approx 0.0045$ . The curves are shown together with the curves for the isothermal case (dashed line) and  $P_4 = 0$  case

approaching the (lower)  $P_4 = 0$  curve in the  $V \rightarrow 1$  limit. If the value of  $P_3$  exceeds  $P_3^*$  (as is the case in both Figs. 11 and 12b), the mobility curve for the isothermal case is *below* the zero- $P_4$  curve, and thus the nonzero- $P_4$  curves always *initially increase* to approach the (higher) curve for the  $P_4 = 0$  case.

Based on the just described behavior of the mobility curves, we expect the kinetic relation to be *always non-monotone* when  $P_3$  is below  $P_3^*$ . See Fig. 12b. The interval of small velocities in which the kinetic relation is *unstable* ( $G(V)$  decreasing) becomes smaller as either  $P_4$  or  $P_3$  increase. When  $P_3$  is above  $P_3^*$ , both monotone and non-monotone curves can be observed. The curves are *monotone* at sufficiently large  $P_4$  at given  $P_1$ . When  $P_1$  is large enough for the kinetic relation at zero  $P_4$  to lose monotonicity, a sufficiently small  $P_4$  results in a *non-monotone* kinetic relation. For example, all mobility curves in Fig. 11a and the curve for  $P_4 = 100$  in Fig. 11b are monotone, but the other curves in Fig. 11b are non-monotone. Observe also that at a given  $P_1$  and small enough  $P_4$  the thermal trapping we have seen for the no-convection case translates into the *non-convexity* of the mobility curves in this case. Indeed, when  $P_4$  is sufficiently small and  $P_3 > P_3^*$ , the driving force rapidly increases at small  $V$  to approach the  $P_4 = 0$  curve from the lower isothermal starting point. Thus the non-monotone mobility curves in this case are not unstable right away: rather, the driving force increases, then decreases and again increases with  $V$  in this case. See, for example, the curves for  $P_4 = 1$  and 10 depicted in Fig. 11b.

Note that when convection is included, the kinetic relation can always be approximated by a linear function at small  $V > 0$ :

$$G = G_r + \alpha V + O(V^2), \quad (60)$$

where the coefficient in the linear term is given by

$$\alpha = \frac{P_1 e_T^2}{16\sqrt{P_4}} \left( 4P_3^2 - \frac{e_T^2}{T_+} \right). \quad (61)$$

at nonzero  $P_4$ . Recalling (46), we observe that  $\alpha < 0$  (driving force initially decreasing) when  $P_3 < P_3^*$  and is positive otherwise. When  $\alpha$  is positive, one can define the so-called *mobility coefficient* for the phase boundaries, given by  $\omega = 1/\alpha$ . This quantity measures how fast the interface will move according to the linearized kinetic

relation. For example, when  $P_4$  tends to zero at  $P_3 > P_3^*$ , the mobility coefficient  $\omega$  tends to zero as well (thermal trapping). As  $P_4$  tends to infinity,  $\omega$  also tends to infinity. Thus the linearized kinetic relation indicates an arbitrary fast propagation of the phase boundary in this case. Our *nonlinear* kinetic relation thus shows the inadequacy of the linearization in this limit.

We note that the approximation (60) *does not* correspond to a so-called “normal growth” assumption frequently postulated in kinetic theories (see [18] for a discussion of this hypothesis), in which  $G$  is *linearly proportional* to  $V$  at small velocities, because in our case  $G_r = G(0+)$  is nonzero. The linearity of the kinetic relation at small  $V$  is, however, in sharp contrast with the no-convection ( $P_4 = 0$ ) kinetic relations, which have a zero initial slope ( $\alpha = 0$ ) and are thus at least *quadratic* (and, at large  $P_1$ , decreasing) functions of  $V$  at small velocities. The incompatibility of the “normal growth” assumption with the non-isothermal kinetic relations that do not include convection was also observed in [17].<sup>2</sup> It is thus interesting to note that while the assumption is also not valid (due to nonzero resistance) in the model that takes convection into account, the relation is approximately *linear* at small  $V$ .

Finally, we remark that previous studies of the effects of heat conduction and convection on the velocity of a propagating phase boundary were conducted in the context of the purely thermal approach [23,24], which is based on the Stefan problem and assumes that the time scale of temperature redistribution is much larger than the time scale of phase transformation and stress relaxation. On this time scale (13)<sub>1</sub> yields the equilibrium equation  $\sigma(w, T) = \text{const}$ . Instead of the viscosity mechanism used here for the internal (mechanical) dissipation, these authors assume that interface does not propagate until the stress in the wire reaches one of the critical values  $\sigma_{\pm} = \sigma_M(T_{\text{int}}) \pm \sigma^{\text{hyst}}$  and then propagates at stress  $\sigma = \sigma_+$  for  $V > 0$  and  $\sigma = \sigma_-$  for  $V < 0$ . Here  $\sigma_M(T_{\text{int}})$  is the (temperature-dependent) Maxwell stress evaluated at the temperature  $T_{\text{int}}$  of the interface, and  $\sigma^{\text{hyst}}$  is the experimentally measured additional stress needed to account for the non-thermal (quasistatic) portion of the hysteresis. Then the energy balance for a traveling wave becomes, in the original variables,

$$c_e \tilde{V} \tilde{T}' = \kappa \tilde{T}'' - \eta(\tilde{T} - \tilde{T}_+) \quad (62)$$

for  $\tilde{z} \neq 0$  (outside the phase boundary), and the the jump condition

$$\llbracket \kappa \tilde{T}' \rrbracket_{\tilde{z}=0} = -l^* \tilde{V} \quad (63)$$

needs to be satisfied across the phase boundary, with

$$l^* = \mu B e_T \tilde{T}_{\text{int}} + \sigma^{\text{hyst}} e_T \quad (64)$$

and  $\tilde{T}_{\text{int}} = \tilde{T}(0)$ . To facilitate comparison with [23], we use the original unrescaled variables and denote these  $\tilde{z}$ ,  $\tilde{T}$  and  $\tilde{V}$  in order to distinguish them from their dimensionless counterparts. Recall that the first term in (64),  $Q_L = \mu B e_T \tilde{T}_{\text{int}}$ , is the latent heat of the transformation. The second term models the instantaneous process of mechanical dissipation. The model yields temperature profiles similar to those depicted in Fig. 10 and, for sufficiently high values of convection coefficient  $\eta$ , can be used to obtain hysteresis loops that are in a good agreement with experiments (see also [2]).

The model considered in this paper is more general because it includes the details of the mechanical dissipation and does not assume instantaneous phase transition. To show how our model can be reduced to the purely thermal model just described, consider the relationship between the velocity  $\tilde{V}$  of the interface and  $\delta \tilde{T} = \tilde{T}_{\text{int}} - \tilde{T}_+$ , the temperature increase at the propagating front. Observing that  $\delta \tilde{T} = C_3 \mu / c_e$  and using (57) with  $\gamma = 0$ , we obtain

$$\delta \tilde{T} \sqrt{(c_e \tilde{V})^2 + 4\eta\kappa} = \tilde{V} \left( B \mu e_T \tilde{T}_{\text{int}} + \frac{\mu e_T^2}{2(1 - V^2)} \right). \quad (65)$$

Observe that the first term inside parentheses on the right-hand side of (65) is the latent heat, while the second equals  $\tilde{G}_{\text{iso}}(V) T_+$ , where  $\tilde{G}_{\text{iso}}(V)$  is the driving force for the isothermal phase transition given by (28). Recall that this driving force equals the signed area between the Rayleigh line and the stress-strain curve (see, for example, (27)). In the purely thermal description of [23] the Rayleigh line reduces to  $\sigma = \sigma_M(\tilde{T}(0)) \pm \sigma^{\text{hyst}}$  for  $\text{sign}(\tilde{V}) = \pm 1$ , and so the second term in parentheses equals  $\sigma^{\text{hyst}} e_T$ . Recalling (64), one can see that the relationship (65) between the temperature increase at the interface and the velocity of the phase boundary becomes

$$\delta \tilde{T} \sqrt{(c_e \tilde{V})^2 + 4\eta\kappa} = \tilde{V} l^*, \quad (66)$$

<sup>2</sup> Note, however, that in the isothermal limit the model considered in [17], which includes a strain-gradient (capillarity) term, is compatible with the “normal growth” approximation - cf [18], while our no-capillarity model is not.

an expression obtained in [23]. Observe that when  $\eta = 0$  (no convection) this yields an *arbitrary* interface velocity at critical stress. This unrealistic conclusion results from oversimplifying the mechanical portion of the dissipation process. The present work includes a more detailed description of the mechanics of phase transitions, and finite values of interface velocity are predicted even when the effects of convection can be neglected.

## 6 Conclusions

In this paper we studied traveling wave solutions in the non-isothermal viscoelastic bilinear model and derived an exact formula describing interface kinetics. The thermal dissipation included both heat conduction and convection mechanisms. Our results for the no-convection case agree with some earlier numerical observations and approximations in [16, 17] for the non-isothermal viscosity-capillarity model, in particular, non-monotonicity of the mobility curve at sufficiently low heat conduction and thermal trapping phenomenon at sufficiently high latent heat. When convection is included, non-monotonicity of the kinetic relation is also observed at small latent heat. The model with convection generalizes the purely thermal model of [23]. We show that in this case mobility curves originate from the isothermal curves but approach the curves for the no-convection case at high velocities. The obtained temperature profiles show localized *self-heating* frequently observed in shape memory alloys during phase transition.

*Acknowledgements.* The author would like to thank P. Rosakis for suggesting the thermoelastic bilinear material law. Helpful discussions with S.-C. Ngan, L. Truskinovsky and S. Turteltaub are also greatly appreciated.

## References

1. Krishnan RV (1985) Stress induced martensitic transformations. *Materials Science Forum*, 3, 387–398
2. Leo PH, Shield TW, Bruno OP (1993) Transient heat transfer effects on the pseudoelastic behavior of shape-memory wires. *Acta Metallurgica et Materialia*, 41(8), 2477–2485
3. Shaw JA, Kyriakides S (1995) On the thermomechanical behavior of NiTi. *Journal of the Mechanics and Physics of Solids*, 43, 1243–1281
4. Shield TW (1995) Orientation dependence of the pseudoelastic behavior of single crystals of Cu-Al-Ni in tension. *Journal of the Mechanics and Physics of Solids*, 43(6), 869–895
5. Ericksen JL (1975) Equilibrium of bars. *Journal of Elasticity* 5, 191–202
6. James RD (1980) The Propagation of Phase Boundaries in Elastic Bars. *Archive for Rational Mechanics and Analysis* 73, 125–157
7. Abeyaratne R, Knowles JK (1993) A continuum model of a thermoelastic solid capable of undergoing phase transitions. *Journal of the Mechanics and Physics of Solids* 41, 541–571
8. Truskinovsky L (1987) Dynamics of nonequilibrium phase boundaries in a heat conducting elastic medium. *Journal of Applied Mathematics and Mechanics (PMM)* 51, 777–784
9. Abeyaratne R, Knowles JK (1991) Implications of viscosity and strain gradient effects for kinetics of propagating phase boundaries in solids. *SIAM Journal on Applied Mathematics* 51, 1205–1221
10. Slemrod M (1983) Admissibility criteria for propagating phase boundaries in a van der Waals fluid. *Archive for Rational Mechanics and Analysis* 81, 301–315
11. Truskinovsky L (1982) Equilibrium interphase boundaries. *Soviet Physics Doklady* 27, 306–331
12. Ngan S-C, Truskinovsky L (2002) Thermo-elastic aspects of dynamic nucleation. *Journal of the Mechanics and Physics of Solids To appear.*
13. Vainchtein A, Rosakis P (1999) Hysteresis and stick-slip motion of the interfaces in dynamic models of phase transitions. *Journal of Nonlinear Science* 9(6), 697–719
14. Slemrod M (1984) Dynamic phase transitions in a van der Waals fluid. *Journal of Differential Equations* 52, 1–23
15. Turteltaub S (1997) Viscosity and strain gradient effects on the kinetics of propagating phase boundaries in solids. *Journal of Elasticity* 46(1), 53–90
16. Ngan S-C (1997) Kinetics of adiabatic phase boundaries and decomposition of metastable states in solids. PhD thesis, University of Minnesota, Minneapolis
17. Ngan S-C, Truskinovsky L (1999) Thermal trapping and kinetics of martensitic phase boundaries. *Journal of the Mechanics and Physics of Solids* 47, 141–172
18. Truskinovsky L (1994) About the “normal growth” approximation in the dynamic theory of phase transitions. *Continuum Mechanics and Thermodynamics* 6, 185–208
19. Vainchtein A (2001) Stick-slip interface motion as a singular limit of the viscosity-capillarity model. *Mathematics and Mechanics of Solids* 6(3), 323–341
20. Rosakis P, Knowles JK (1998) Unstable kinetic relations and the dynamics of solid-solid phase transitions. *Journal of the Mechanics and Physics of Solids* 45, 2055–2081
21. Rosakis P, Knowles JK (1999) Continuum models for irregular phase boundary motion in shape-memory tensile bars. *European Journal of Mechanics Part A Solids* 18, 1–16
22. Webb TW, Aifantis EC (1995) Oscillatory fracture in polymeric materials. *International Journal of Solids and Structures* 32, 2725–2743

23. Bruno OP, Leo PH, Reitich F (1995) Free boundary conditions at austenite-martensite boundary. *Physical Review Letters* 74(5), 746–749
24. Malomed BA, Rumanov EN (1985) Natural velocity of the boundary between phases. *Soviet Physics Doklady* 30(10), 872–874
25. Fedelich B, Zanzotto G (1992) Hysteresis in discrete systems of possibly interacting elements with a two well energy. *Journal of Nonlinear Science* 2, 319–342
26. Truskinovsky L (1985) Structure of an isothermal phase jump. *Soviet Physics Doklady* 30, 945–948
27. Patashinskii AZ, Chertkov MV (1990) Motion of a front of a phase transition under strong supercooling conditions. *Soviet Physics of Solid State* 36, 295–299
28. Umansev A (1992) Thermodynamic stability of phases and transition kinetics under adiabatic conditions. *Journal of Chemical Physics* 96, 605–617